Civil and Environmental Engineering
Vol. 0, Issue 0, DOI: 10.2478/cee-2027-0038

Investigating the Performance of Rehabilitated Non-Prismatic Reinforced Concrete Columns Subjected to Cyclic Load

Romaih O. MOSTAFA[1,*], Sofyan Y. AHMED[1], Jasim A. ABDULLAH[1]

[1] Civil Engineering Department, University of Mosul, Mosul, Iraq.

* corresponding author: romaih.23enp54@student.uomosul.edu.iq

Date of Submission: 02 September 2026
Revision Date: 23 September 2026
Date of Acceptance: 24 September 2026

Civil and Environmental Engineering
Journal of the Faculty of Civil Engineering | University of Žilina

Abstract

The cyclic performance and post-damage rehabilitation of non-prismatic reinforced concrete columns, remain insufficiently characterized. This study investigates the axial, pushover, and cyclic behaviour of non-prismatic RC columns and evaluates two rehabilitation techniques-ferrocement jacketing and steel-plate jacketing-applied after yield-level damage. Eight non-prismatic columns were fabricated and tested. Two control specimens were loaded axially to failure to establish load-carrying capacity; two underwent pushover testing at 20% and 40% axial load ratios to determine yield displacement; and four were subjected to yield-level reversed cyclic loading to induce controlled permanent deformation, then repaired with a 25 mm ferrocement jacket or a 2.71 mm steel-plate jacket and retested under quasi-static cyclic protocol. The columns achieved an average axial capacity of 905 kN and failed in shear at the necking region. Increasing the axial loading ratio from 20% to 40% reduced the yield displacement from 7.35 mm to 5.7 mm (22.5%) and lowered dissipated hysteretic energy by approximately 21%, while increasing lateral strength by 86%. Both rehabilitation techniques effectively restored strength and stiffness: steel jacketing delivered partial stiffness recovery and higher performance levels, whereas ferrocement delivered full stiffness recovery and dissipated marginally more energy (9% higher at 20% axial load). Increasing the sustained load from 20% to 40% narrows the difference of the total energy dissipated in both types of rehabilitation. Steel jacketing is the preferable choice where residual-drift control is the governing design criterion, while ferrocement remains a viable, more economical alternative where moderate ductility demand and lower axial load ratios are expected.

Keywords

Non-prismatic columns; Reinforced concrete; Rehabilitation; Ferrocement jacketing; Steel jacketing; Cyclic loading.

1. Introduction

Non-prismatic reinforced concrete columns-structural elements with systematically varying cross-sections along their height-represent a critical component in modern infrastructure, particularly in seismic regions. These columns, also termed tapered or variable-section columns, are extensively employed in bridge piers, tall structures, and specialized architectural applications where structural efficiency and aesthetic considerations converge. The structural behaviour of non-prismatic columns differs fundamentally from that of prismatic elements due to the continuous variation in stiffness and strength along the member length.

© Author(s) 2026. This work is distributed under the Creative Commons BY 4.0 license (https://creativecommons.org/licenses/by/4.0/).

Analytical design methods for non-prismatic reinforced concrete columns have evolved to address the unique challenges posed by variable cross-sections, including non-uniform stiffness distribution, complex moment-curvature relationships, and the need to account for second-order effects in slender members. Traditional design approaches developed for prismatic columns require significant modification to accurately predict the behaviour of tapered elements(Head & Aristizabal-Ochoa, 1987; Aghayere, 1990; Manzelli & Harik, 1993).

Non-prismatic reinforced concrete columns find extensive application in bridge and infrastructure systems, where they serve as primary vertical load-bearing elements in substructures. The use of tapered columns in bridges is motivated by structural efficiency, aesthetic considerations, and the need to accommodate varying load demands along the column height(Poston et al., 1986; Saiidi et al., 1998; Darwish et al., 1996; Wehbe & Saiidi, 1999).

Experimental testing of tapered columns under axial load has shown that increasing the longitudinal reinforcement ratio and providing adequate transverse ties markedly raise load capacity and reduce lateral displacement, while hollow sections reduce ultimate capacity substantially relative to solid ones (Al-Maliki & Mahmood, 2018; Al-Maliki et al, 2021). Under lateral loading, this variation in section properties complicates the prediction of plastic hinge location: push-over analyses of RC columns with structural flares indicate that hinge position is strongly governed by the longitudinal steel arrangement rather than occurring reliably at the member end (Wehbe & Saiidi, 1999).

Retrofit research on non-prismatic columns remains comparatively limited. External jacketing techniques—using steel or ferrocement jackets—significantly enhance the seismic performance, shear capacity, and displacement ductility of reinforced concrete (RC) columns (Abdullah & Takiguchi, 2003; Chai, Y. H., et al., 1991; Li et al., 2005). However, current design codes offer little specific guidance for non-prismatic members, since most provisions were developed for prismatic elements (Kadhim & Al-Zaidee, 2024; Aghayere, 1990). This gap is significant because ferrocement and steel jacketing are widely used, cost-effective repair techniques for conventional RC members, yet their comparative effectiveness in restoring the stiffness, strength, and energy-dissipation capacity of damaged non-prismatic columns has not been established experimentally.

A consideration that has received limited explicit attention in this literature is the geometric consequence of jacketing when the member is tapered. Jackets are surface-applied, they modify the cross-sectional dimensions along the member; for a linearly tapered column, a jacket of constant thickness preserves the taper slope but reduces the taper ratio and increases flexural rigidity. Such interventions preserve, attenuate, or eliminate the non-prismatic character of the member is rarely reported, which complicates comparison between studies.

This study addresses that gap by experimentally investigating the axial, pushover, and cyclic behaviour of non-prismatic RC columns, and by evaluating two rehabilitation techniques – ferrocement jacketing and steel-plate jacketing – applied after yield-level cyclic damage. The objectives are: (i) to establish the axial load-carrying capacity and failure mechanism of non-prismatic columns; (ii) to investigate the push-over response of exposed (without jacketing) specimens those are initially applied to two ratios of axially loading (20 & 40%) & determine their yield displacement; and (iii) to compare the two rehabilitation techniques in terms of strength recovery, stiffness restoration, and dissipated energy under the quasi-static cyclic protocol. It is hypothesized that the sustained axial load ratio governs both the yield displacement and the dissipated energy of the non-prismatic columns, and that steel-plate and ferrocement jacketing each restore seismic performance to a different degree, with steel jacketing providing greater stiffness recovery and ferrocement offering comparable ductility at lower cost.

2. Methodology

2.1. Research Design

This study adopts an experimental research design, comprising laboratory-based physical testing of non-prismatic reinforced concrete columns. The experimental program was conducted in five sequential phases: axial loading to failure, pushover testing under sustained axial load, controlled reversed cyclic loading to induce yield-level damage, application two rehabilitation techniques (ferrocement or steel-plate jacketing) under a 20% or 40% axial load ratio, and post-rehabilitation reversed cyclic loading following the quasi-static protocol. The rehabilitation phase follows a repeated-measures, pre–post intervention arrangement, with jacketing type and axial load ratio as the primary controlled variables.

2.2. Materials and Procedures

2.2.1. Materials

Ordinary Portland cement (Type I), sourced from Sinjar Co. Ltd. (Nineveh, Iraq), served as the primary binder and satisfied the physical and chemical limits of Iraqi Specification IQS 5/2018 (Central Organization for Standardization and Quality Control [COSQC], 2018a). River sand conforming to Zone 2 grading requirements (fineness modulus = 2.79) was used as fine aggregate, and rounded river gravel with a 12.5 mm maximum size served as coarse aggregate; both complied with IQS 45/2018 (COSQC, 2018b). Mixing water met the potability requirements of IQS 1703/2018 (COSQC, 2018). The concrete mix was proportioned to yield a measured 28-day compressive strength of f'c = 28.5 MPa, and a splitting tensile strength of 2.35 MPa.

Deformed steel bars (ϕ10 mm main reinforcement, ϕ8 mm stirrups) conforming to ISO 6935-2-2019 for grade B500B-R and B300D-R respectively were used. Tensile testing showed an average yield strength of 627 MPa and 307 MPa for two respective diameters.

Two rehabilitation materials were characterized. The ferrocement jacket (25 mm thickness, two layers of steel wire mesh at 1.8% volume fraction and specific surface of 0.053mm2/mm3 complied with ACI 549.1R-18 requirements) used a one-component, polymer-modified, fibre-reinforced repair mortar (Cempatch S) manufactured by Don Construction Products (DCP), with mechanical properties(fc =41.3 MPa @ 14days, modulus of rupture fr= 6.96 MPa @ 14 days) complied with EN 12190, ASTM C348, and ASTM C307; the wire mesh itself was tested per ACI 549.1R-18 (ACI Committee 549, 2018), yielding a tensile strength of 772 MPa. The steel-plate jacket used a 2.71 mm sheet with an average yield stress of 327 MPa, verified by tensile testing per ASTM E8 (ASTM International, 2022); the gap between the jacket and the column was filled with a low-viscosity epoxy resin (Quickmast 105 manufactured by DCP) which has a compressive strength more than 70 MPa, flexural strength more than 45 MPa, and tensile strength more than 25 MPa. A carbon-fibre-reinforced polymer (CFRP) wrap of characteristics shown in Table 1 was additionally applied at both column ends over a length of 150 mm to confine these regions and solely to prevent premature local bearing failure and did not form part of the rehabilitation variables under investigation.

Table 1: The mechanical properties of the Profiber CW300

Brand	Weight [g/m^2]	Design thickness [mm]	Tensile strength [MPa]	Tensile E-modulus [GPa]	Elongation at break [%]
DCP PROFIBER CW300	300	0.166	4800	230	1.7

2.2.2. Specimen Design

Eight non-prismatic RC columns (150 mm depth, tapered width, 1500 mm height) were fabricated, the longitudinal reinforcement was selected to meet the ACI 318-25 minimum requirements, a ratio ranging from 1% at the ends to 2.09% at mid height (6 ϕ10 mm bars) and transverse reinforcement detailed per ACI 318-25 §18.4.3.3 (ACI Committee 318, 2025) – ϕ8 mm stirrups at 75 mm spacing over the end 250 mm regions and at 140 mm spacing over the mid-length as shown in Figure 1. Because it is difficult to cast the formworks vertically in the laboratory, the samples were cast while lying flat on a level surface. The specimens were assigned to three experimental groups: two for axial loading to failure (NPRIS-0, NPRIS-1), two for pushover testing (LA20, LA40, at 20% and 40% of axial capacity, respectively), and four for pre-damage cyclic loading followed by rehabilitation (FJLA20, FJLA40, SJLA20, SJLA40).

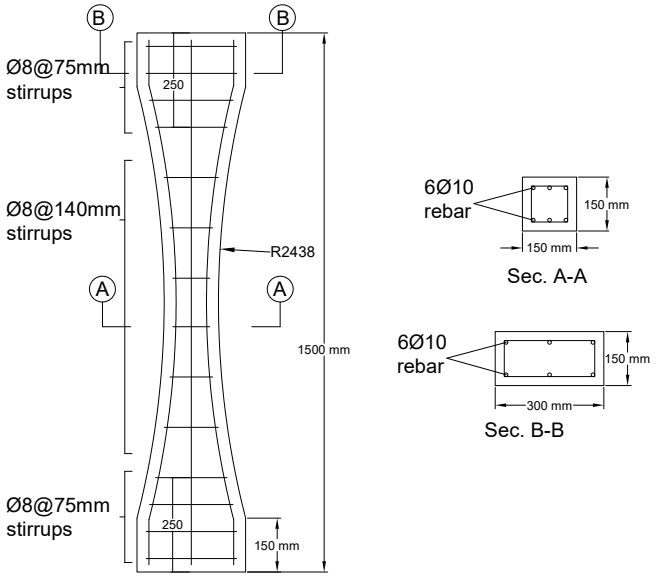


Figure 1: Geometry of the non-prismatic test specimen of columns



Figure 2: Fabrication of the specimens

2.2.3. Instrumentation and Test Setup

Axial loads were applied using a compression testing machine of 1500 kN capacity, with a load cell mounted on the hydraulic jack. Lateral cyclic and pushover loads were applied through a transverse hydraulic jack supported by a dedicated steel reaction frame rigidly connected to the main frame. Axial and lateral displacements were recorded using linear variable differential transformers (LVDTs), and strain in the longitudinal bars and stirrups was monitored using high-sensitivity general-purpose strain gauges (118.5 ± 0.5 Ω, ±5% strain range). All load cells, LVDTs, and strain gauges were connected to a 16-channel data logger (TDS-530), recording at one sample per second throughout each test. The boundary conditions included a fixed constraint at the base, which was achieved by encasing the column in a heavy steel cover that was secured to the ground with six M14 bolts. The fixed length along the column's longitudinal axis was 150 mm. To ensure high friction between the column and the cap, an additional 0.8-mm-thick sheet was inserted between them. Additionally, four M14 bolts were placed on each side of the cap to ensure complete contact between the sheet and the column. A similar cap is installed at the upper end of the column to prevent translation and rotation permitting displacement only in the direction of lateral loading and producing double-curvature bending.

2.2.4. Test Procedure

Specimen preparation: Molds were fabricated from 18 mm plywood as illustrated in Figure 2. Reinforcement cages were assembled, instrumented with strain gauges at designated locations, and placed with 25 mm cover spacers before casting. Concrete was mixed for 3 minutes per batch (sufficient for two columns), and each specimen was compacted using vertical vibration for 3–5 seconds per position.

Axial loading test, following alignment and instrumentation, the two designated specimens (NPRIS-0, NPRIS-1) were loaded concentrically to failure to establish load-carrying capacity and failure mode as shown in Figure 3.



Figure 3: Performing specimens test to axial loading

Pushover test, the two designated specimens were first loaded axially to a sustained ratio (20% or 40% of capacity), after which lateral load was applied at a low rate until it exceeds the ultimate load displacement, and the flexural stiffness drops into the degrading region. The lateral load is applied in the direction along the weak axis of the column as such axis is

most vulnerable to deformation during earthquake events. According to the study performed by R. Park (Park, 1989),the yield displacement (Δy) was subsequently determined from each load–displacement curve using the elastic–perfect-plastic idealization. The approach assumes an elasto-plastic model. this model is consists of elastic linear part starting from the origin point passing through the point of 40% of ultimate load and go up to the ultimate load level. Then the model continues as perfect plastic part. The yield deformation point (Δy) is the yield point formed in this model. Figure (4 and 5) show the instrumentation arrangement of the pushover test.

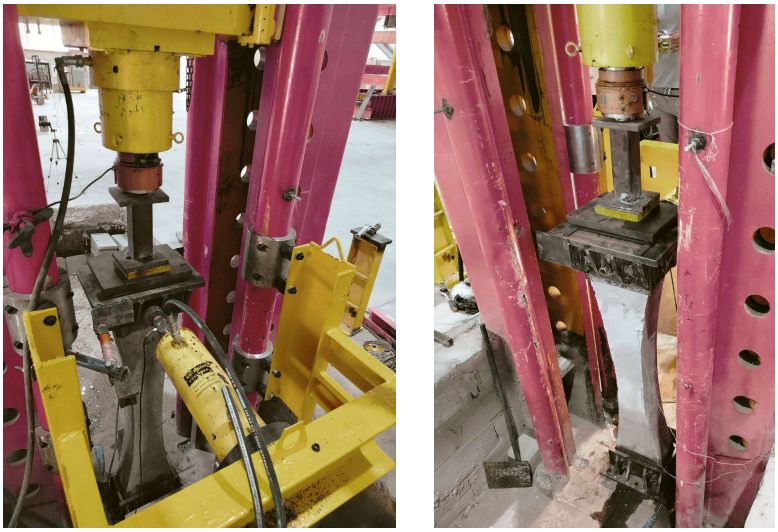


Figure 4: Instrumentation arrangement of the lateral loading

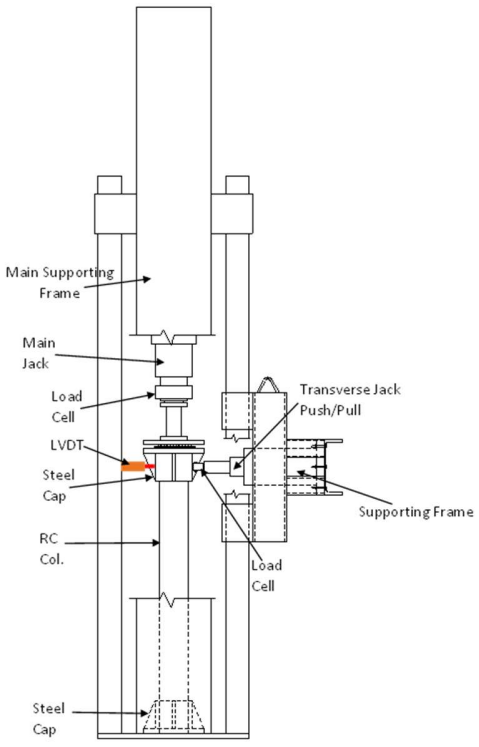


Figure 5: Layout of the testing rig

Pre-rehabilitation cyclic loading. The four remaining specimens were subjected to reversed cyclic lateral displacement under their respective sustained axial loads, following a four-cycle protocol (two cycles at 0.5Δy, and two cycles at Δy) intended to induce a controlled, repeatable level of permanent yield damage suitable for subsequent repair.

Rehabilitation application. Ferrocement jacketing was applied by installing the wire mesh directly onto the damaged column surface, followed by hand-plastering of the Cempatch S mortar to a 25 mm thickness as shown in Figure 6. After that, 14-day moist curing under wet jute fabric was applied. Steel-plate jacketing was applied by cutting and welding four steel sheets around the column as shown in Figure 7 using E7018 welding rod of yielding strength fy=390MPa, sealing the jacket ends with polyurethane sealant and filling the resulting gap between the jacket and the concrete with low-viscosity epoxy resin to ensure a full contact.



Figure 6: Rehabilitation using ferrocement jacketing



Figure 7: Rehabilitation using steel jacketing

Post-rehabilitation cyclic loading. corresponding to defined structural performance levels (operational (OP), immediate occupancy (IO), life safety (LS), and collapse prevention (CP)) accordance with ACI 374.2R-13 shown in Table 2. The rehabilitated specimens were retested under their original sustained axial load and a displacement-controlled reversed cyclic proposed protocol shown in Figure 8., Table 3., and Table 4., comprising seven progressively increasing displacement

amplitudes (0.5Δy through 6Δy, two cycles each). The bottom end of the column was fully restrained (fixed) by a stiff steel cap over a distance of 150mm. Therefore, the drift ratio is obtained based on a column height of 1350mm.

Table 2: The performance levels according to ACI-374-2R-13 in terms of the drift ratio

Drift status	Performance level			
	OP operational	IO immediate occupancy	LS life safety	CP collapse prevention
Transient drift (temporary)	<<1%	≤1%	≤2%	≤4%
Permanent drift (residual)	<<1%	<1%	≤1%	≤4%

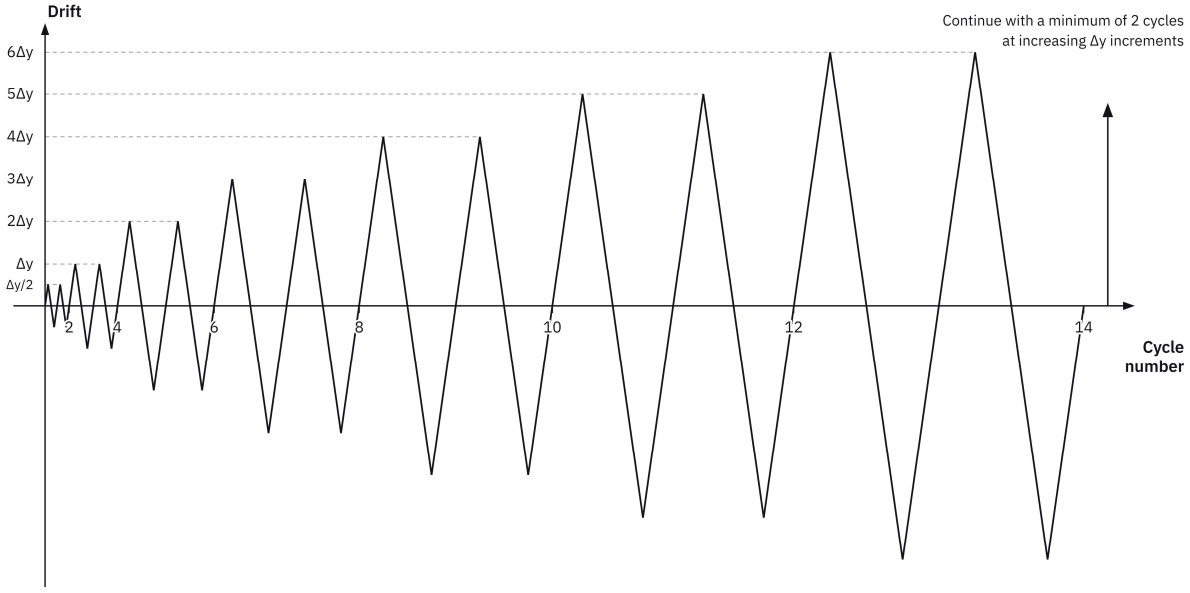


Figure 8: Cyclic loading history

Table 3: Protocol imposed on specimens (FJLA20 & SJLA20) in terms of performance level

Cycle No.	Amplitude	Displacement [mm]	Drift ratio [%]	Transient performance level
1	0.5Δy	3.7	0.27	IO
2	Δy	7.4	0.54	IO
3	2Δy	14.8	1.09	LS
4	3Δy	22.2	1.64	LS
5	4Δy	29.6	2.19	CP
6	5Δy	37.0	2.74	CP
7	6Δy	44.4	3.28	CP

Table 4: Protocol imposed on specimens (FJLA40 & SJLA40) in terms of performance level

Cycle No.	Amplitude	Displacement [mm]	Drift ratio [%]	Transient performance level
1	0.5Δy	2.9	0.21	IO
2	Δy	5.7	0.43	IO
3	2Δy	11.4	0.84	IO
4	3Δy	17.1	1.26	LS
5	4Δy	22.8	1.68	LS
6	5Δy	28.5	2.11	CP
7	6Δy	34.2	2.53	CP

2.3. Data Collection

Data collection in this study was instrument-based and quantitative, generated directly through physical testing. accordingly, this section instead details specimen allocation, the instrumentation used to acquire data, the parameters recorded, and the timing/frequency of data capture across each test phase, consistent with reporting conventions for experimental structural engineering studies.

In addition to the instrumented quantitative record, visual inspection was performed at each load increment throughout testing. Crack initiation, propagation, and final failure pattern were documented photographically and by manual annotation directly on the specimen surface, with the corresponding load level recorded at each stage. This visual record supported interpretation of the failure mode (e.g., shear failure localized at the necking region) and complemented the instrumented data in identifying the onset of damage.

3. Results

experimental outcomes obtained from the physical testing of eight non-prismatic reinforced concrete (RC) columns, cover four sequential phases: (i) axial loading to failure, (ii) pushover testing under sustained axial load, (iii) pre-rehabilitation reversed cyclic loading used to induce a controlled level of yield damage, and (iv) post-rehabilitation reversed cyclic loading of the ferrocement- and steel-plate-jacketed specimens. Each set of findings is followed by an engineering interpretation of the underlying structural mechanism and, where directly comparable prior research exists, a discussion of how the present results align with, extend, or diverge from previously published studies on non-prismatic and tapered reinforced concrete columns. All results presented are drawn exclusively from the experimental program.

3.1. Axial Load-Carrying Capacity and Failure Mode

The two non-prismatic specimens (NPRIS-0, NPRIS-1) were tested under monotonic concentric compression reached an average maximum axial load of 905.1 kN (Table 5). Both specimens failed in shear, with the failure plane consistently localized at the reduced mid-height (necking) region rather than distributed randomly along the member as shown in Figure 9. Figure 10 Shows the axial behaviour of the tested specimens. It is noted that, there is a difference or shift between the curves although they belong to identical specimens. This phenomenon is common in concrete, and it is attributed to many reasons such as the coarse aggregate orientation and interlock, the concentration of coarse aggregate, the location where the yielding begins, and the stress flow path. Reinforcement strain at maximum load remained below the calculated yield strain of the longitudinal bars (0.0031), indicating that the main reinforcement had not yet yielded at the point of peak axial load; yielding occurred only after the load peak was reached.

Table 5: Axial load test results for non-prismatic RC columns

Description	NPRIS-0	NPRIS-1	Average
Max. load [kN]	854.4	955.8	905.1
Axial displ. at max load [mm]	3.036	3.86	3.448
Strain in the rebar at max load	-0.0027	-0.0028	-0.00275
Strain in the stirrup at max load	0.0014	0.0015	0.00145
Axial stiffness [kN/m]	312,100	349,649	330,874
Toughness [J]	1047.5	1577	1312



Figure 9: Shear failure mode in non-prismatic specimens

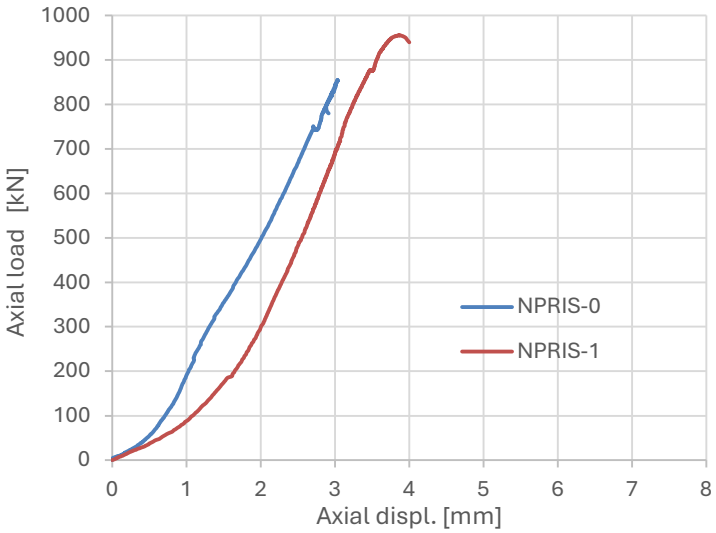


Figure 10: Axial load – deflection curves for NPRIS-0 & NPRIS-1

3.2. Pushover Response and Yield Displacement

The two specimens (LA20, LA40) tested under combined sustained axial load and monotonic lateral push exhibited yield displacements of 7.35 mm and 5.70 mm under 181kN (20%) and 362kN (40%) axial load ratios as listed in Table 6 and the pushover behaviour is shown in Figure 11. Both specimens developed cracks gradually in the upper and lower regions of the columns on opposite faces, as shown in Figure 12. The cracks were parallel and perpendicular to the column's longitudinal axis. Cracks were observed at high levels of lateral loading before reaching the ultimate load. No cracks were noticed in the necking zone. The location and the orientation of the cracks indicate that the flexural failure mode is dominant. First visible cracks occurred at a higher lateral load (45 kN under 40% versus 34 kN under 20%). The test results state that raising the sustained axial load ratio from 181kN to 362kN reduced the yield displacement by approximately 22%, and the ductility factor (μd) by 44% while nearly doubling the yield load (Py), from 17.2 kN to 32.0 kN.

Table 6: Pushover test results (yield and ductility parameters)

Specimen	Axial load	Δy [mm]	Py [kN]	Δu [mm]	μd = Δu/Δy
LA20	20% (181 kN)	7.35	17.2	62.6	8.52
LA40	40% (362 kN)	5.70	32.0	27.43	4.80

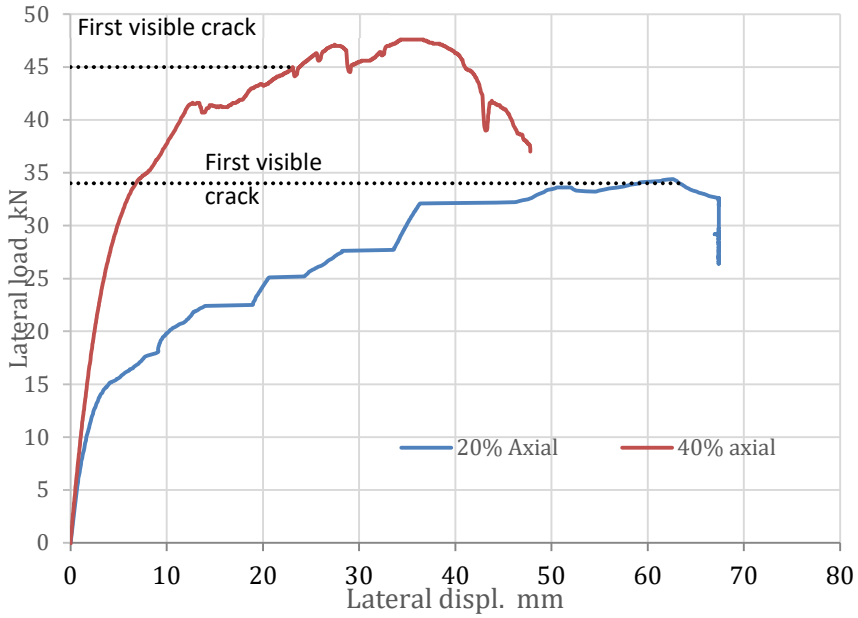


Figure 11: Pushover behaviour under 20% & 40% axial load

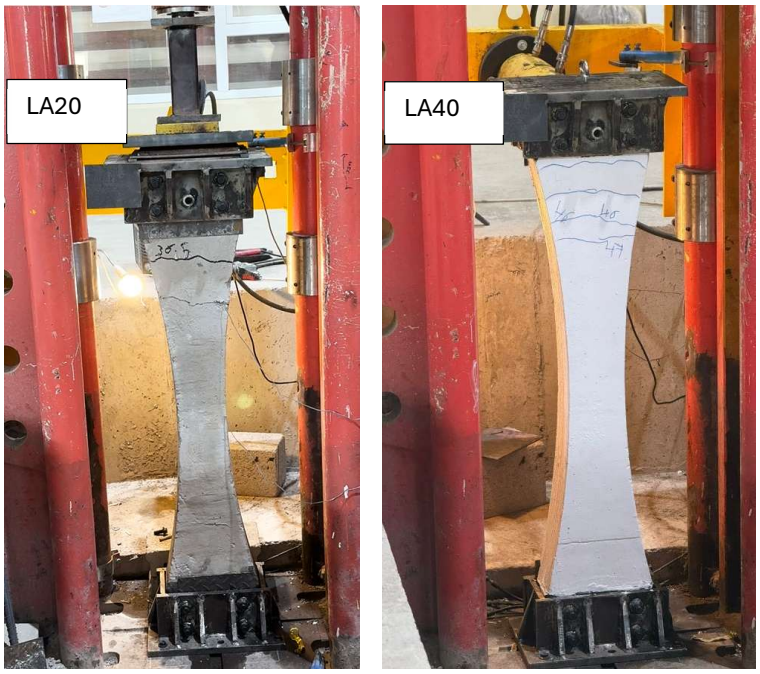


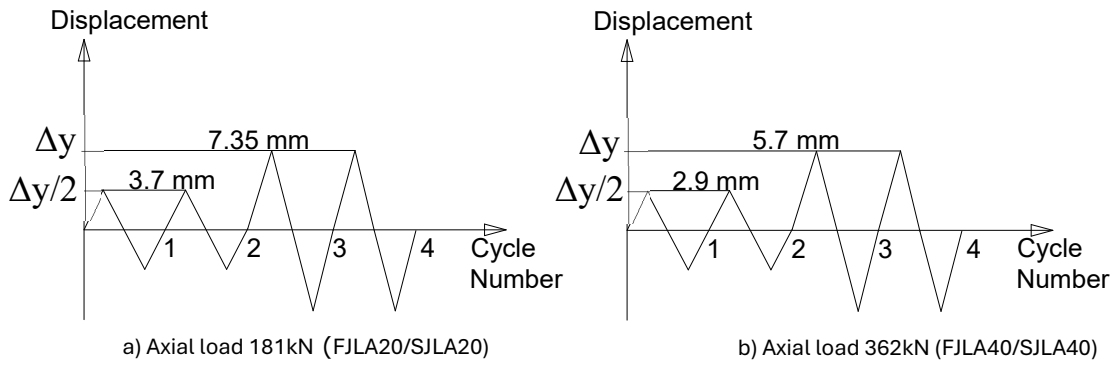
Figure 12: Cracking pattern in the specimens LA20 & LA40 after pushover test

3.3. Pre-rehabilitation Cyclic Loading (Damage Induction)

Prior to rehabilitation, the four designated specimens were subjected to reversed cyclic displacement at 0.5Δy and Δy (two cycles each) as shown in Figure 13. to induce a controlled, repeatable level of permanent damage. The cumulative dissipated energy recorded over these four cycles is summarized in Table 7. The dissipated energy is represented by the area enclosed by hysteresis loops. Given the existence of hundreds of points for each cycle, these areas have been calculated based on Gauss's Area Formula (shoelace formula). The recorded hysteresis loops are shown in Figure 14 through Figure 17. Figure 18 illustrates the cumulative dissipated energy by the four specimens as a comparison chart.

Table 7: Dissipated energy prior to the rehabilitation (kN·mm)

Specimen	Cycle 1 [0.5Δy]	Cycle 2 (0.5Δy)	Cycle 3 (Δy)	Cycle 4 (Δy)	Total
FJLA20	62.12	45.66	145.28	108.51	361.57
SJLA20	38.72	30.88	131.53	100.65	301.78
FJLA40	37.14	23.43	127.28	82.71	270.56
SJLA40	35.43	25.46	131.38	63.67	255.94



a) Axial load 181kN (FJLA20/SJLA20) b) Axial load 362kN (FJLA40/SJLA40)

Figure 13: Displacement protocol imposed on test specimens before rehabilitation

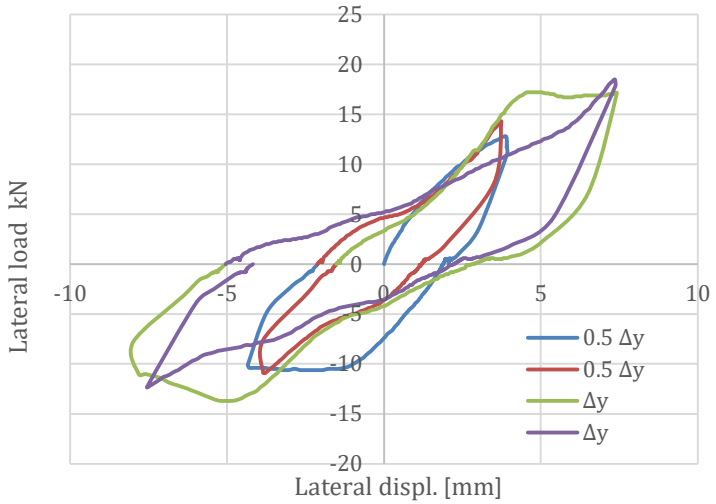


Figure 14: Cyclic behaviour of FJLA20 specimen under 181kN axial load

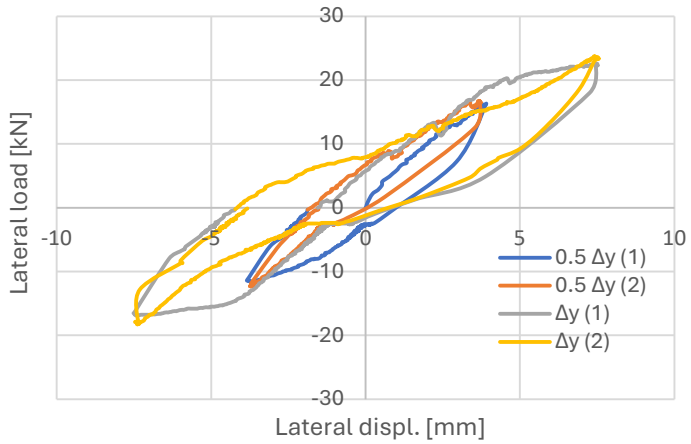


Figure 15: Cyclic behaviour of SJLA20 specimen under 181kN axial load

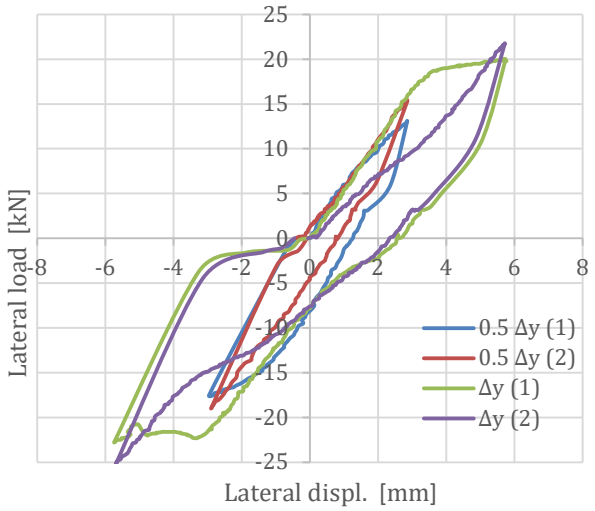


Figure 16: Cyclic behaviour of FJLA40 specimen under 362kN axial load

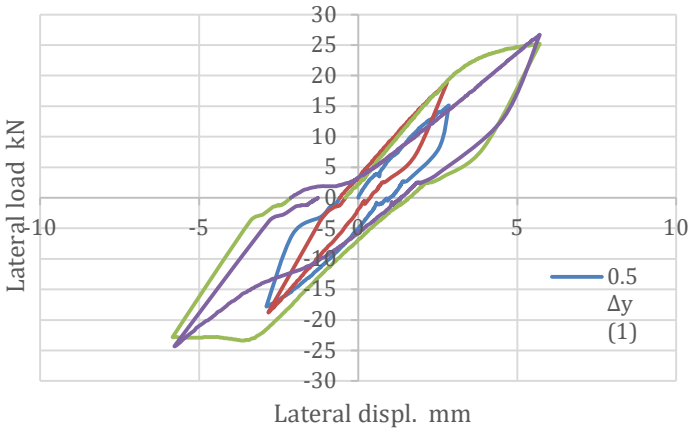


Figure 17: Cyclic behaviour of SJLA40 specimen under 362kN axial load

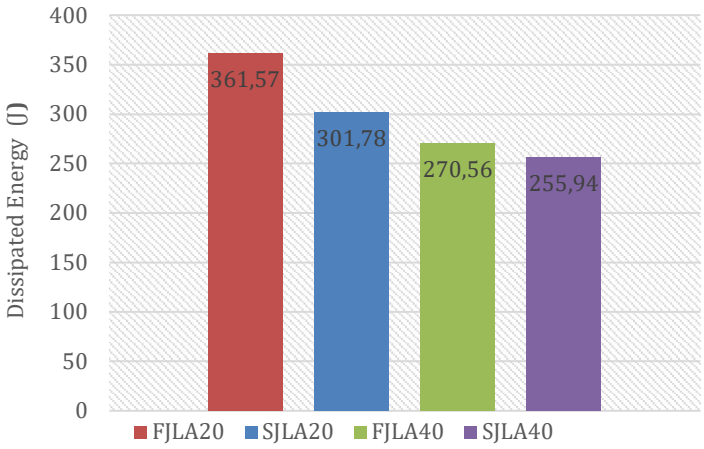


Figure 18: Pre rehabilitation dissipated energy

3.4. Post-rehabilitation Cyclic Response and Performance Levels

Following jacketing, the four specimens were retested under displacement-controlled protocol, comprising seven progressively increasing amplitude levels (0.5Δy to 6Δy, two cycles each). Table 8 summarizes the cumulative dissipated energy for each jacketing technique and axial load ratio, and Table 9 summarizes the residual (permanent) deformation used to classify each specimen's post-rehabilitation structural performance level. Figures (19, 20, 21, 22) show the hysteresis loops of the rehabilitated specimens.

Table 8: Cumulative dissipated energy after rehabilitation (kN.mm)

Axial load ratio	Ferrocement jacket	Steel-plate jacket	Difference (ferrocement vs. steel)
20%	8,927.8	8,188.2	+9.0%
40%	8,084.6	8,034.8	+0.6%

Table 9: Residual deformation and resulting performance-level classification

Specimen	Permanent deformation at final cycle [mm]	Performance level
FJLA20	21.14	Collapse prevention (CP)
FJLA40	19.88	Collapse prevention (CP)
SJLA20	10.41	Life safety (LS)
SJLA40	12.79	Collapse prevention CP (close to Life safety boundary)

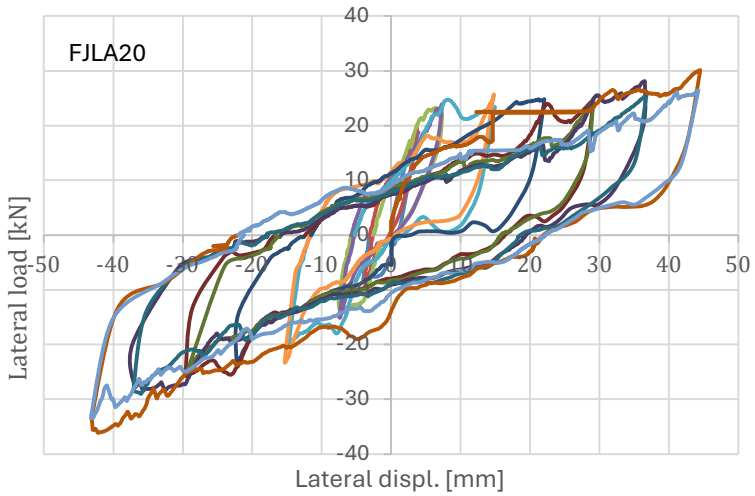


Figure 19: Hysteresis loops for FJLA20 after the rehabilitation

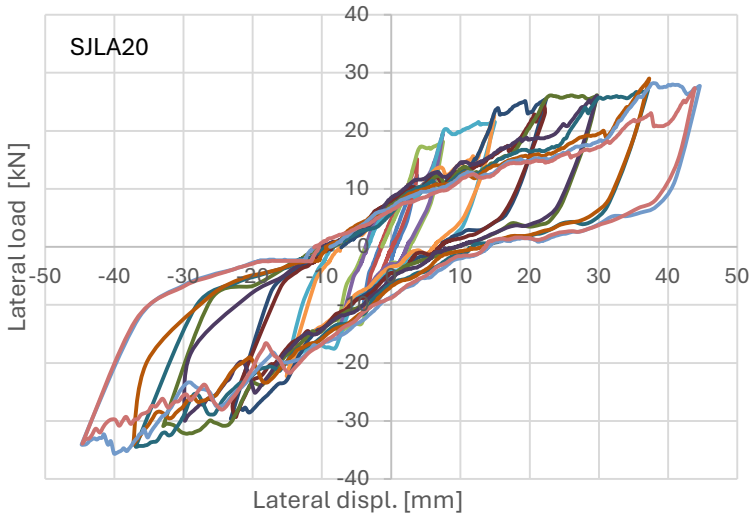


Figure 20: Hysteresis loops for SJLA20 after the rehabilitation

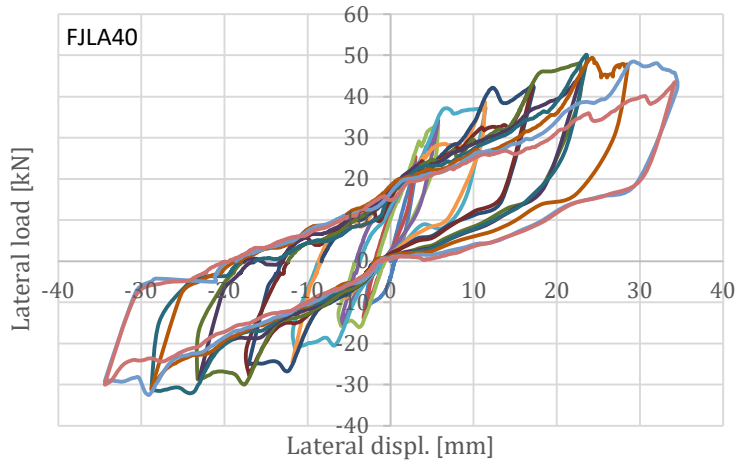


Figure 21: Hysteresis loops for FJLA40 after the rehabilitation

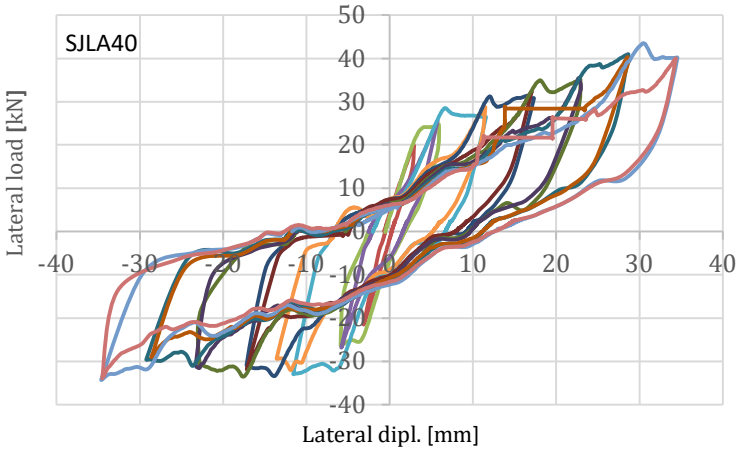


Figure 22: Hysteresis loops for SJLA40 after the rehabilitation

3.5. The Effect of Jacketing on the Flexural Stiffness

Jacketing in general increases the cross-sectional area of the column, resulting in greater stiffness. Figure 23 shows the cyclic behaviour of the specimens before and after the rehabilitation. The monotonic pushover behaviour, the final cycle (fourth) of Damage Induction stage (BefRehdy(2)), and the first cycle of loading of post rehabilitation stage (AftReh0.5dy(1)) placed together in a single diagram to study the effect of jacketing on the stiffness.

It is clear from Figure 23 that the flexural stiffness of the rehabilitated specimens has been restored compared to the deformed specimens before rehabilitation. This is evidence of jacketing efficiency. On the other hand, the comparison of flexural stiffness between rehabilitated specimens' behaviour and the pushover curve indicates that the specimens (FJLA20 & FJLA40) of ferrocement jacketing have totally restored the initial stiffness, while the specimen (SJLA20 & SJLA40) restored it partially.

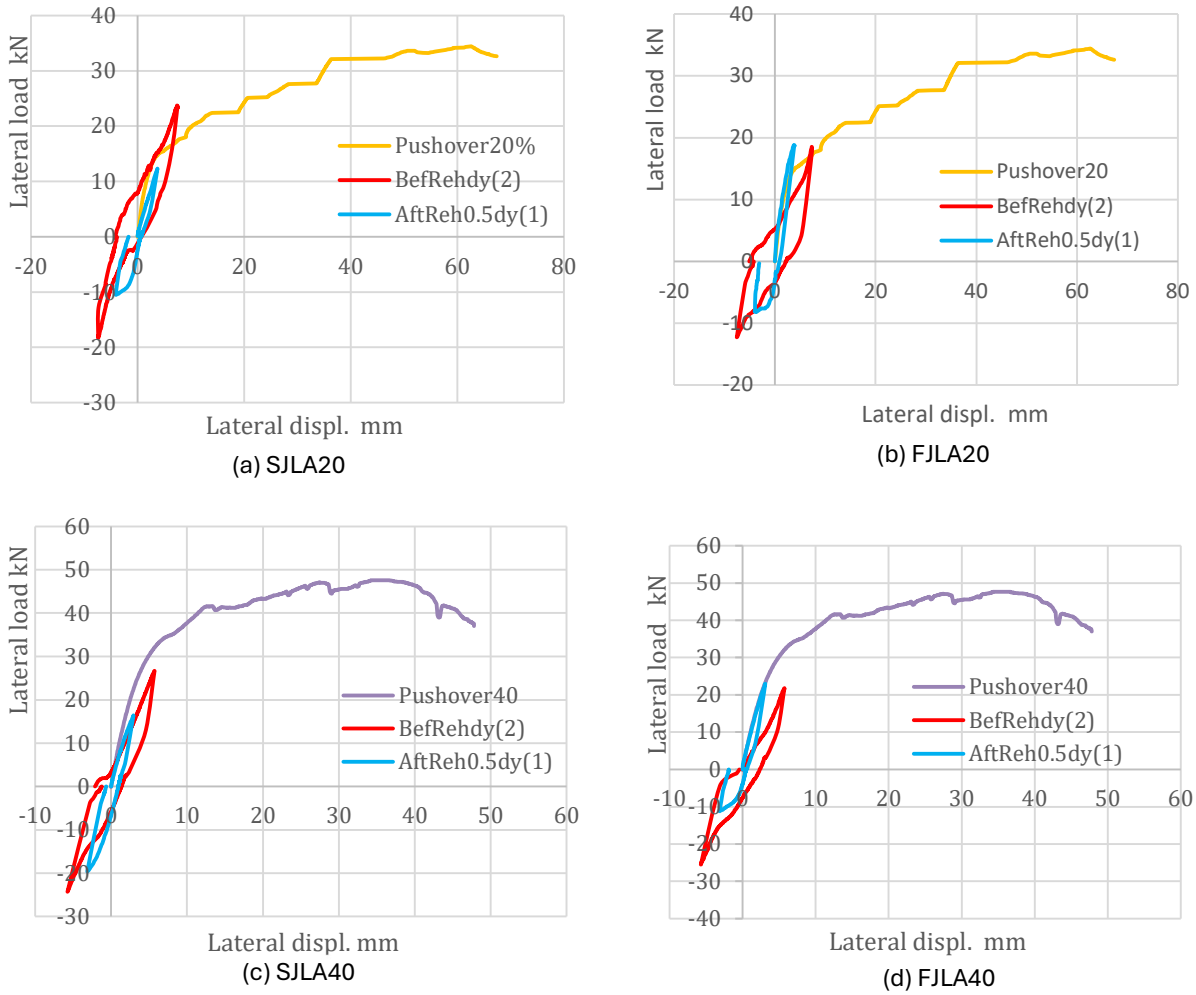


Figure 23: Comparison among pushover, damaged induction, and post rehabilitation response

4. Discussion

4.1. Interpretation of Results

4.1.1. Behaviour of the Columns under the Axial Loading

The observed localization of shear failure at the necking region is attributable to the strut-and-tie action inherent to the non-prismatic geometry (He et al., 2014). The enlarged end sections act as bearing zones that distribute the concentrated stresses imposed by the testing machine more uniformly into the column core, while the reduced mid-height section concentrates compressive and shear stress, forming the critical section of the member. In addition, the geometry subjects the concrete in the mid-height region to a biaxial stress condition that delays the onset of microcracking and internal collapse relative to a uniformly stressed prismatic section, a phenomenon documented in the concrete-mechanics literature (Kupfer et al., 1969).

4.1.2. Behaviour of the Columns under the Pushover Effect

The reduction in yield displacement, coupled with the increase in yield load under higher sustained axial load, reflects a compressive stiffening effect: the sustained axial force keeps flexural cracks tightly closed under low-amplitude lateral loading, effectively raising the flexural stiffness of the section and delaying the onset of visible cracking. This is consistent with the direct proportionality between axial load and lateral flexural stiffness identified in the testing program. However, this same stiffening effect reduces deformation capacity, explaining the lower ductility ratio (μd=4.80) at 40% of load-carrying capacity than at 20% (μd=8.52). The sensitivity of tapered-column stiffness and cracking behaviour to axial load ratio observed here parallels findings reported for other non-prismatic configurations. Kadhim and Al-Zaidee (Kadhim et al., 2025) demonstrated that tapering RC columns by reducing cross-sectional concrete volume can enhance the seismic performance of RC frame structures when the geometry is properly proportioned relative to the demand, a conclusion consistent with the present finding that the column's stiffness and yield response are highly sensitive to the applied load level.

4.1.3. Induction the Damage into the Columns

Combining specimens by axial load ratio, the total average energy dissipated under 40% axial load (263.250 kN.mm) diminishes by 21% compared to the 20% axial load (331.675 kN.mm). This reduction is consistent with the P-Δ (P-delta) mechanism described in ACI 374.2R-13 (*ACI 374.2R-13*, n.d.): under a higher sustained axial load, the secondary moment generated by lateral displacement consumes a larger proportion of the section's total moment capacity, accelerating strength degradation and leaving less capacity available for hysteretic energy dissipation at a given displacement amplitude.

4.1.4. Rehabilitation Techniques

At the 20% axial load ratio, the ferrocement-jacketed specimen (FJLA20) dissipated 9% more hysteretic energy than its steel-jacketed counterpart (SJLA20) but also exhibited approximately double the residual deformation (21.14 mm versus 10.41 mm), placing it at a lower (more damaged) performance level. At the 40% axial load ratio, the two jacketing techniques dissipated nearly identical total energy (a 0.6% difference), while the steel-jacketed specimen again showed markedly lower residual deformation (12.79 mm versus 19.88 mm). This pattern is explained by the differing confinement mechanisms of the two jacket systems. The ferrocement jacket relies on closely spaced, relatively small-diameter wire meshes embedded in a polymer-modified mortar; this distributed, semi-flexible reinforcement permits a greater degree of incremental micro-cracking within the jacket itself before failure, which increases hysteretic energy dissipation but also allows a larger irrecoverable (permanent) drift to accumulate. The steel-plate jacket, in contrast, forms a continuous, high-stiffness confining shell bonded to the column with epoxy resin; this continuous confinement more effectively restrains lateral

expansion of the damaged concrete core, limiting residual drift and providing superior post-cyclic stiffness recovery, at the cost of dissipating marginally less energy under the lower axial load ratio.

The general principle that external jacketing restores seismic performance representing in flexural stiffness in non-prismatic columns after cyclic damage is corroborated by the limited existing retrofit literature for this column type. (Martinovic et al., 2000) conducted dynamic testing of non-prismatic RC bridge columns retrofitted with fibre-reinforced polymer (FRP) jackets and found that jacketing enhanced seismic performance by providing external confinement and increasing shear capacity, a mechanism directly analogous to the confinement action of both the ferrocement and steel jackets evaluated in the present study, despite the difference in jacket material. This convergence across independently tested jacket materials (FRP, ferrocement, and steel) suggests that external confinement is a generally effective rehabilitation principle for non-prismatic columns, irrespective of the specific jacketing material selected. The present comparison between ferrocement and steel further extends this literature by quantifying a material-dependent trade-off between energy dissipation and residual-drift control that has not been previously reported for non-prismatic sections. This trade-off is consistent with the broader finding of Guadagnuolo et al. (Guadagnuolo et al., 2020) that the type, amount, and pitch of transverse confining reinforcement significantly affects confined-concrete behaviour; the continuous steel jacket in the present study functions similarly to a closely spaced, continuous confinement detail, while the ferrocement mesh functions similarly to a more distributed but comparatively less continuous confinement detail, consistent with the superior residual-drift control observed for the steel-jacketed specimens. The present results also respond directly to a research gap identified in the literature: current design codes provide little specific guidance for non-prismatic members, since most provisions were developed for prismatic elements (Aghayere, 1990; Kadhim & Al-Zaidee, 2024), and comprehensive rehabilitation procedures for non-prismatic columns using economical materials such as ferrocement or steel plate have not been systematically evaluated in the literature prior to this study.

4.2. Limitations

Each test condition in this program was represented by a single specimen rather than replicate specimens. Accordingly, the quantitative comparisons reported above should be interpreted as indicative structural trends rather than statistically validated differences.

5. Conclusion

This study experimentally investigated the axial, pushover, and cyclic behaviour of eight non-prismatic reinforced concrete columns and evaluated the effectiveness of ferrocement jacketing versus steel-plate jacketing in restoring seismic performance following yield-level cyclic damage. Based on the experimental program, the following conclusions are drawn:

Axial capacity and failure mode. The tested non-prismatic columns achieved an average axial load-carrying capacity of approximately 905 kN, with shear failure consistently localized at the reduced mid-height (necking) region in both specimens. This confirms that the tapered geometry reliably governs the failure location, concentrating structural vulnerability at a predictable, inspectable section rather than distributing it randomly along the member.

Effect of axial load ratio on pushover response. Increasing the sustained axial load ratio from 20% to 40% of capacity reduced the yield displacement by roughly 22% and the ductility factor by 44% while nearly doubling the yield lateral load. This indicates that sustained axial compression produces a measurable stiffening effect that trades deformation capacity for load capacity, and that yield displacement – and therefore the design of any subsequent cyclic protocol — cannot be assumed independent of the axial load level.

Effect of axial load ratio on cyclic energy dissipation. Prior to the rehabilitation, the hysteretic energy dissipated under 40% axial load is less than that dissipated under 20% axial load by approximately 21%. This confirms that axial load

ratio is a primary variable governing cyclic degradation in non-prismatic columns, independent of any subsequent rehabilitation.

Effectiveness of rehabilitation. Both ferrocement and steel-plate jacketing successfully restored post-damage seismic performance to at least the Life Safety level under the ACI 374.2R-13 classifications, confirming that external jacketing is an effective, generalizable rehabilitation strategy for non-prismatic RC columns damaged under cyclic load.

Ferrocement versus steel-plate jacketing. The two techniques exhibited a consistent trade-off across both axial load ratios tested: steel-plate jacketing produced markedly lower residual (permanent) deformation and therefore post-cyclic stiffness recovery, while ferrocement jacketing, in addition to restoring the initial stiffness effectively, dissipated marginally more hysteretic energy at the lower (20%) axial load ratio, though this energy-dissipation advantage narrowed to negligible at the higher (40%) ratio. Steel jacketing is therefore the preferable choice where residual-drift control is the governing design criterion, while ferrocement remains a viable, more economical alternative where moderate ductility demand and lower axial load ratios are expected.

Acknowledgements

The authors gratefully acknowledge the Department of Civil Engineering, University of Mosul, for providing the academic and administrative support necessary to carry out this work.

Sincere thanks are extended to the staff of the Construction Materials Testing Laboratory, Department of Civil Engineering, University of Mosul, for their technical assistance and for making the testing equipment and facilities available throughout the experimental program.

Finally, the authors thank the administration of the College of Engineering, University of Mosul, for their support in facilitating this research.

Author Contributions

R.O.M. conducted the experimental testing, collected and analysed the data, and drafted the original manuscript. **S.Y.A.** conceived and designed the study, contributed to the methodology design, supervised the research, and reviewed and edited the manuscript. **J.A.A.** conceived and designed the study, contributed to the methodology design, supervised the research, and reviewed and edited the manuscript. All authors have read and approved the final version of the manuscript.

Disclosure of Interest

The authors declare that they have no known competing financial interests or personal relationships that could have appeared to influence the work reported in this paper.

Data Availability Statement

The data supporting the findings of this study are available from the corresponding author upon reasonable request.

References

Abdullah, & Takiguchi, K. (2003). An investigation into the behavior and strength of reinforced concrete columns strengthened with ferrocement jackets. Cement and Concrete Composites, 25(2), 233–242. https://doi.org/10.1016/S0958-9465(02)00005-7.

ACI Committee 374. (2013). Guide for testing reinforced concrete structural elements under slowly applied simulated seismic loads (ACI 374.2R-13). American Concrete Institute.

Aghayere, A. D. (1990). Design of Nonprismatic Concrete Columns by the Degree of Fixity Method. ACI Structural Journal, 87(4). https://doi.org/10.14359/3099.

Al-Maliki, H. N. G. (2021). NONLINEAR SIMULATION ANALYSIS OF TAPERED REINFORCED CONCRETE COLUMN (SOLID AND HOLLOW) BEHAVIOR UNDER AXIAL LOAD. International Journal of GEOMATE, 21(86). https://doi.org/10.21660/2021.86.j2295.

Al-Maliki, H. N. G., & Mahmood, M. S. (2018). Structural Behavior Investigation of Reinforced Concrete Tapered Solid and Hollow Section Columns under Axial Load. Association of Arab Universities Journal of Engineering Sciences, 25(2), 1–18.

Chai, Y. H., Priestley, M. J. N., & Seible, F. (1991). Seismic Retrofit of Circular Bridge Columns for Enhanced Flexural Performance. ACI Structural Journal, 88(5). https://doi.org/10.14359/2759.

Darwish, I., Saiidi, M. S., & Sanders, D. H. (1996). CCEER-96-3: Seismic Retrofit of R/C Oblong Tapered Bridge Columns with Inadequate Bar Anchorage in Columns and Footings. http://hdl.handle.net/11714/7228.

Guadagnuolo, M., Donadio, A., Tafuro, A., & Faella, G. (2020). Experimental Behavior of Concrete Columns Confined by Transverse Reinforcement with Different Details. The Open Construction & Building Technology Journal, 14(1), 250–265. https://doi.org/10.2174/1874836802014010250.

He, Z.-Q., Liu, Z., & Ma, Z. J. (2014). Explicit Solutions of Transverse Tensions in Deep Beams: Load-Path Model and Superposition Principle. ACI Structural Journal, 111(3). https://doi.org/10.14359/51686575.

Head, M. C., & Aristizabal-Ochoa, J. D. (1987). Analysis of Prismatic and Linearly Tapered Reinforced Concrete Columns. Journal of Structural Engineering, 113(3), 575–589. https://doi.org/10.1061/(ASCE)0733-9445(1987)113:3(575).

Kadhim, J. A., & Al-Zaidee, S. R. (2024). Numerical Simulation for Strength and Stability of RC Tapered Columns. Engineering, Technology & Applied Science Research, 14(4), 14819–14824. https://doi.org/10.48084/etasr.7228.

Kadhim, J. A., Al.Zaidee, S. R., & Al-Baghdadi, H. A. (2025). Seismic Performance of Reinforced Concrete Non-Prismatic Columns. Journal of Engineering, 31(7), 53–69. https://doi.org/10.31026/j.eng.2025.07.03.

Kupfer, H., Hilsdorf, H. K., & Rusch, H. (1969). Behavior of Concrete Under Biaxial Stresses. ACI Journal, 66(8), 656-666. https://doi.org/10.14359/7388.

Li, Y., Hwang, J., Chen, S., & Hsieh, Y. (2005). A study of reinforced concrete bridge columns retrofitted by steel jackets. Journal of the Chinese Institute of Engineers, 28(2), 319–328. https://doi.org/10.1080/02533839.2005.9670997.

Manzelli, A. A., & Harik, I. E. (1993). Prismatic and Nonprismatic Slender Columns and Bridge Piers. Journal of Structural Engineering, 119(4), 1133–1149. https://doi.org/10.1061/(ASCE)0733-9445(1993)119:4(1133).

Martinovic, F., Saiidi, M. S., Sanders, D. H., & Gordaninejad, F. (2000). CCEER-00-4: Dynamic Testing of Non-Prismatic Reinforced Concrete Bridge Columns Retrofitted with FRP Jackets. http://hdl.handle.net/11714/7265.

Park, R. (1989). Evaluation of ductility of structures and structural assemblages from laboratory testing. Bulletin of the New Zealand Society for Earthquake Engineering, 22(3), 155–166. https://doi.org/10.5459/bnzsee.22.3.155-166.

Poston, R. W., Diaz, M., & Breen, J. E. (1986). Design Trends for Concrete Bridge Piers. ACI Journal Proceeding, 83(1). https://doi.org/10.14359/10739.

Saiidi, M., Maragakis, E., & Sanders, D. (1998). Evaluation and seismic retrofit of highway bridge substructures with tapered columns. Construction and Building Materials, 12(2–3), 161–173. https://doi.org/10.1016/S0950-0618(97)00018-4

Wehbe, N., & Saiidi, M. (1999). Seismic Vulnerability of Reinforced Concrete Columns with Structural Flares. ACI SP 187-13: Seismic Response of Concrete Bridges, 275-297. https://doi.org/10.14359/5603.

How to Cite This Article

O. Mostafa, R., Y. Ahmed, S., & A. Abdullah, J. (2026). Investigating the Performance of Rehabilitated Non-Prismatic Reinforced Concrete Columns Subjected to Cyclic Load. Civil and Environmental Engineering, 0 (0). https://doi.org/10.2478/cee-2027-0038